Green's Function Models and Measurements for Body Area Network (BAN) Channels

Ahmed M. Eid, Noman Murtaza, and Jon W. Wallace*

Jacobs University Bremen, School of Engineering and Science
Campus Ring 1, 28759 Bremen, Germany, PH: +49 421 200 3197
E-mail: a.eid@jacobs-university.de, noman.murtaza@tu-ilmenau.de, wall@ieee.org

I. INTRODUCTION

In wireless body area networks (BANs), communicating nodes are present near, directly on, or inside the body. Designing high-performance BAN systems is challenging due to competing goals of high capacity, minimal interference, robustness, and low power consumption. Since the body forms an integral part of the communications channel and near-field environment of the antennas, traditional antenna design specifications may no longer apply, complicating the antenna design problem, but also opening new research opportunities.

One approach for characterizing BAN propagation is to model or measure the channel in realistic environments [1], [2], where body propagation, antenna characteristics, and scattering from nearby objects are all lumped into the channel, leading to site- and antenna-specific descriptions. A more general approach is to develop BAN models that capture propagation effects due to the *body alone*, allowing arbitrary antennas and environments to be described with a single model. Also, where possible, BAN models should be kept as simple as possible to allow easy implementation and rapid simulation.

This work investigates using the spatially varying Green's function of an idealized body to provide a model that is independent of the antennas and scattering environment. Similar to [3], this paper considers a lossy infinite circular cylinder model for the body, but generalized to include arbitrary source and observation polarization. Additionally, measurements are performed in a compact anechoic chamber with non-resonant short monopoles, better approximating an ideal point current source and field sensor. The results indicate that the simple model is adequate for certain polarizations, but insufficient for others. Also, this effort reveals some practical limitations of BAN measurements in compact chambers.

II. CIRCULAR CYLINDER MODEL

The body is modeled as a lossy circular dielectric cylinder centered at the origin with (complex) permittivity ϵ_{r1}, radius a, and infinite extent in the z direction, embedded in an infinite medium with relative permittivity ϵ_{r2}. Wave number and intrinsic impedance for region i are k_i and η_i, respectively. The cylinder is excited with a line current $\mathbf{J}$ centered at polar coordinates $\rho = \rho'$ and $\phi = \phi'$

$$\mathbf{J} = (a_\rho \hat{\rho}' + a_\phi \hat{\phi}' + a_z \hat{z}) \exp(-jk_z z), \tag{1}$$

where the sinusoidal variation in z is included to allow a line-to-point transformation as well as model oblique far-field plane wave sources. Vector potential of incident field is $\mathbf{A}_{\text{inc}} = -\mu H_0^{(2)}(k_{\rho 2} R)/(4j)\mathbf{J}$, or

$$\mathbf{A}_{\text{inc}} = -\frac{\mu}{4j} H_0^{(2)}(k_{\rho 2} R)\{\hat{\rho}[a_\rho \cos(\phi-\phi') + a_\phi \sin(\phi-\phi')] + \hat{\phi}[a_\phi \cos(\phi-\phi') - a_\rho \sin(\phi-\phi')] + \hat{z}a_z\} \exp(-jk_z z), \tag{2}$$

where $k_z^2 + k_{\rho i}^2 = k_i^2$ and $R = \sqrt{\rho^2 + \rho'^2 - 2\rho\rho'\cos(\phi-\phi')}$. To obtain homogeneous boundary conditions at the surface of the scatterer, the source is expanded in terms of polar functions centered at the origin (cylinder axis) using

$$H_0^{(2)}(k_{\rho 2} R) = \sum_n \underbrace{H_n(k_{\rho 2}\rho')J_n(k_{\rho 2}\rho)}_{F_n}\underbrace{\exp[jn(\phi - \phi')]}_{Q_n}, \tag{3}$$

where $H_n(x) = H_n^{(2)}(x)$. Incident electric field is $E_{\text{inc}} = \omega/(jk_2^2)[\nabla(\nabla \cdot \mathbf{A}_{\text{inc}}) + k_2^2\mathbf{A}_{\text{inc}}]$, or

$$\mathbf{E}_{\text{inc}} = -j\frac{\eta_2}{8k_2}\sum_n\left\{\hat{\rho}\left(T_n' + k_2^2 X_n\right) + \hat{\phi}\left(\frac{jn}{\rho}T_n + k_2^2 Y_n\right) + \hat{z}j\left(2k_2^2 a_z F_n - k_z T_n\right)\right\}\Psi, \tag{4}$$

where $\Psi = e^{-jk_z z}e^{jn(\phi-\phi')}$,

$$T_n = X_n' + \frac{X_n}{\rho} + j\frac{n}{\rho}Y_n + 2k_z a_z F_n, \qquad X_n = F_{n-1}(a_\phi + ja_\rho) + F_{n+1}(-a_\phi + ja_\rho),$$

$$Y_n = F_{n-1}(-a_\rho + ja_\phi) + F_{n+1}(a_\rho + ja_\phi), \qquad F_n = H_n(k_{\rho 2}\rho')J_n(k_{\rho 2}\rho). \tag{5}$$

Incident magnetic field is $\mathbf{H}_{\text{inc}} = 1/(2j\mu)(\nabla \times \mathbf{A}_{\text{inc}})$, or

$$\mathbf{H}_{\text{inc}} = \frac{1}{8}\sum_n \left[\hat\rho\left(-\frac{2n}{\rho}a_z F_n + jk_z Y_n\right) + \hat\phi(-jk_z X_n - 2ja_z F_n') + \hat z\left(Y_n' + \frac{1}{\rho}Y_n - \frac{jn}{\rho}X_n\right)\right]\Psi. \tag{6}$$

Next we consider scattered field outside the cylinder and total field inside the cylinder. Due to $e^{-jk_z z}$ variation, transverse electric and magnetic field can be expressed in terms of z-directed field alone, or

$$\mathbf{E}_T = -\frac{j}{k_\rho^2}\left(k\eta\nabla_T \times \hat z H_z + k_z\nabla_T E_z\right), \qquad \mathbf{H}_T = \frac{j}{k_\rho^2}\left(\frac{k}{\eta}\nabla_T \times \hat z E_z - k_z\nabla_T H_z\right). \tag{7}$$

Inside the scatterer, arbitrary total E_z and H_z are represented as

$$E_{z,1} = \sum_n A_n J_n(k_{\rho 1}\rho)\Psi, \qquad H_{z,1} = \sum_n B_n J_n(k_{\rho 1}\rho)\Psi, \tag{8}$$

where scalars A_n and B_n remain to be determined. Substituting (8) into (7) results in

$$\mathbf{E}_{T,1} = -\frac{j}{k_{\rho 1}^2}\sum_n\left\{\hat\rho\left[\frac{jnk_1\eta_1}{\rho}B_n J_n(k_{\rho 1}\rho) + k_z k_{\rho 1}A_n J_n'(k_{\rho 1}\rho)\right] + \hat\phi\left[\frac{jnk_z}{\rho}A_n J_n(k_{\rho 1}\rho) - k_1\eta_1 k_{\rho 1}B_n J_n'(k_{\rho 1}\rho)\right]\right\}\Psi$$

$$\mathbf{H}_{T,1} = \frac{j}{k_{\rho 1}^2}\sum_n\left\{\hat\rho\left[\frac{jnk_1}{\eta_1\rho}A_n J_n(k_{\rho 1}\rho) - k_z k_{\rho 1}B_n J_n'(k_{\rho 1}\rho)\right] + \hat\phi\left[-\frac{jnk_z}{\rho}B_n J_n(k_{\rho 1}\rho) - \frac{k_1 k_{\rho 1}}{\eta_1}A_n J_n'(k_{\rho 1}\rho)\right]\right\}\Psi. \tag{9}$$

Outside the scatterer, arbitrary outward traveling scattered field can be represented as

$$E_{z,2} = \sum_n C_n H_n(k_{\rho 2}\rho)\Psi, \qquad H_{z,2} = \sum_n D_n H_n(k_{\rho 2}\rho)\Psi. \tag{10}$$

Substituting, we have

$$\mathbf{E}_{T,2} = -\frac{j}{k_{\rho 2}^2}\sum_n\left\{\hat\rho\left[\frac{jnk_2\eta_2}{\rho}D_n H_n(k_{\rho 2}\rho) + k_z k_{\rho 2}C_n H_n'(k_{\rho 2}\rho)\right] + \hat\phi\left[\frac{jnk_z}{\rho}C_n H_n(k_{\rho 2}\rho) - k_2\eta_2 k_{\rho 2}D_n H_n'(k_{\rho 2}\rho)\right]\right\}\Psi$$

$$\mathbf{H}_{T,2} = \frac{j}{k_{\rho 2}^2}\left\{\hat\rho\left[\frac{jnk_2}{\eta_2\rho}C_n H_n(k_{\rho 2}\rho) - k_z k_{\rho 2}D_n H_n'(k_{\rho 2}\rho)\right] + \hat\phi\left[-\frac{jnk_z}{\rho}D_n H_n(k_{\rho 2}\rho) - \frac{k_2 k_{\rho 2}}{\eta_2}C_n H_n'(k_{\rho 2}\rho)\right]\right\}\Psi. \tag{11}$$

The unknown coefficients A_n, B_n, C_n, and D_n are found by equating total E_z, H_z, E_ϕ, and H_ϕ on the boundary at $\rho = a$ for each n to obtain

$$A_n J_{n1} = \frac{j\eta_2}{8k_2}\left[jk_z T_n - k_2^2 2ja_z F_n\right] + C_n H_{n2} \tag{12}$$

$$\frac{j}{k_{\rho 1}^2}\left[\frac{jnk_z}{a}A_n J_{n1} - k_1\eta_1 k_{\rho 1}B_n J_{n1}'\right] = \frac{j\eta_2}{8k_2}\left[\frac{jnT_n}{a} + k_2^2 Y_n\right] + \frac{j}{k_{\rho 2}^2}\left[\frac{jnk_z}{a}C_n H_{n2} - k_2\eta_2 k_{\rho 2}D_n H_{n2}'\right] \tag{13}$$

$$B_n J_{n1} = \frac{1}{8}\left[Y_n' + \frac{1}{a}Y_n - \frac{jn}{a}X_n\right] + D_n H_{n2} \tag{14}$$

$$\frac{j}{k_{\rho 1}^2}\left[-\frac{jnk_z}{a}B_n J_{n1} - \frac{k_1 k_{\rho 1}}{\eta_1}A_n J_{n1}'\right] = \frac{1}{8}\left[-jk_z X_n - 2ja_z F_n'\right] + \frac{j}{k_{\rho 2}^2}\left[-\frac{jnk_z}{a}D_n H_{n2} - \frac{k_2 k_{\rho 2}}{\eta_2}C_n H_{n2}'\right], \tag{15}$$

where $H_{ni} = H_n(k_{\rho i}a)$ and $J_{ni} = J_n(k_{\rho i}a)$. For each n, a matrix equation of the form $\mathbf{Z}[A_n B_n C_n D_n]^T = [E_{z,\text{inc},n} E_{\phi,\text{inc},n} H_{z,\text{inc},n} H_{\phi,\text{inc},n}]^T$ is formed and inverted to obtain the unknown coefficients.

Computing incident field for $\rho = \rho'$ with (3) is difficult due to singular behavior. Instead, incident field can be computed directly based on (2). Assuming a line current at the origin in Cartesian coordinates $\mathbf{J} = (\hat x a_x + \hat y a_y + \hat z a_z)\exp(-jk_z z)$, vector potential of the radiated field is given by

$$\mathbf{A}_{\text{inc}} = -\frac{\mu}{4j}(\hat x a_x + \hat y a_y + \hat z a_z)H_0^{(2)}(k_{\rho 2}R)\exp(-jk_z z), \tag{16}$$

where $R = \sqrt{x^2 + y^2}$. We can find $\mathbf{E}_{\text{inc}}$ directly as

$$E_{x,\text{inc}} = \frac{\eta_2}{4k_2} \left\{ a_x \left[\left(H_0^{(2)\prime}(k_{\rho 2}R) + \frac{x^2}{R}U \right) \frac{k_{\rho 2}}{R} + k_2^2 H_0^{(2)}(k_{\rho 2}R) \right] + \frac{a_y k_{\rho 2} xy U}{R^2} - j\frac{xk_z k_{\rho 2} a_z}{R} H_0^{(2)\prime}(k_{\rho 2}R) \right\} e^{-jk_z z}$$

$$E_{y,\text{inc}} = \frac{\eta_2}{4k_2} \left\{ a_y \left[\left(H_0^{(2)\prime}(k_{\rho 2}R) + \frac{y^2}{R}U \right) \frac{k_{\rho 2}}{R} + k_2^2 H_0^{(2)}(k_{\rho 2}R) \right] + \frac{a_x k_{\rho 2} xy U}{R^2} - j\frac{yk_z k_{\rho 2} a_z}{R} H_0^{(2)\prime}(k_{\rho 2}R) \right\} e^{-jk_z z}$$

$$E_{z,\text{inc}} = \frac{\eta_2}{4k_2} \left\{ (k_2^2 - k_z^2) a_z H_0^{(2)}(k_{\rho 2}R) - j\frac{k_z k_{\rho 2}}{R}(xa_x + ya_y) H_0^{(2)\prime}(k_{\rho 2}R) \right\} e^{-jk_z z}, \tag{17}$$

where $U = k_{\rho 2} H_0^{(2)\prime\prime}(k_{\rho 2}R) - (1/R) H_0^{(2)\prime}(k_{\rho 2}R)$. Note that the expression should be translated from the origin to the polar coordinate (ρ', ϕ').

III. Anechoic Chamber Measurements

A small anechoic chamber was constructed for performing on-body measurements having dimensions 2.0 m for the width and length and 2.2 m for the height. The floor was constructed as an open lattice of thin planks, allowing microwave absorber to be placed between the planks and a human subject to stand over the absorber. The walls, floor, and ceiling are covered with EPP-22 absorber material from Telemeter Electronic GmbH, having a guaranteed normal reflection below -40 dB in the 2-4 GHz band. Due to budget constraints, only the center $1.5\text{m} \times 1.5\text{m}$ area of each surface was covered with absorber, which is estimated to be sufficient to remove the strongest specular wall reflections. Figure 1(a) depicts the inside of the chamber with the human subject. Measurements were performed using a Rohde & Schwarz ZVB20 vector network analyzer with the transmit and receive antennas connected to the two ports and 20 dBm transmit power. Although channels were measured with a broadband 2 to 5 GHz sweep, only the results at 2.55 GHz are presented here.

Figure 1(b) and (c) depict the antennas that were used for the measurement, which are 1.5 cm monopoles. The monopoles were intentionally chosen to be short (approximately $\lambda/8$) compared to the wavelength λ at 2.55 GHz, thus approximating a point transmit current and a point receive field sensor. The matching efficiency of the short monopoles is between 0.1 and 0.5 depending on the orientation relative to the body, but we estimate that the maximum additional link loss of 20 dB does not significantly hinder the short range BAN measurements.

Antennas were mounted on the body by sewing them onto small Velcro patches and attaching these to an ordinary back-support Velcro band worn around the waist, as depicted in Figure 1(a). To allow all combinations of the three transmit and receive polarizations to be measured, two antennas were constructed with right angle cable connections ($\hat{\rho}$ polarization) and two with straight connections ($\hat{\phi}$ and $\hat{z}$ polarization). A long Velcro measuring tape was also constructed, which when attached to the waist strap allowed the antennas to be positioned with ± 1 mm accuracy. The subject placed his hands over his head during the measurements to reduce the influence of the arms. Also, the subject stood nearly in the center of the chamber, but with the body turned $30°$ relative to the wall.

Initially, measurements were performed with the network analyzer outside of the chamber connected to the antennas via 3 m SMA cables (Mini-Circuits CBL-10FT-SMS+), referred to as Setup A. Although sufficient in some cases, we found that when the signal was severely obstructed, calibration errors could overshadow the effects we wished to study. In Setup B, measurements were performed by placing the network analyzer in the chamber (covered with absorber) directly in front of the subject with instrument quality 50 cm test cables, allowing a more accurate calibration.

In the following study, one antenna was placed above the left hip of the subject and the other antenna starting above the right hip and moved in 1 cm increments around the waist toward the other antenna. When the antennas were very close (<3 cm), accurate placement was difficult due to the overlap of the Velcro bands, so some variation from the ideal response is expected. The circumference of the subject from the two extreme points above the hip was 47 cm. The thickness of the clothes and Velcro band together was estimated as 0.5 cm. The additional displacement of the antennas from the body was 1.5 cm for $\hat{\rho}$ oriented and 0.5 cm for $\hat{z}$ and $\hat{\phi}$ oriented monopoles.

IV. Representative Results

The radius of the cylinder in the model was chosen to be $a = 14.5$ cm, which gives the same half circumference as the subject (47 cm) when the clothes' thickness is included. Relative permittivity $\epsilon_{r1} = 45.5 - j10.9$ was chosen to match average properties of fat (15%) and muscle (85%) at 2.55 GHz. Computations were performed using $N = 80$ modes to ensure good convergence, even in strongly shadowed cases.
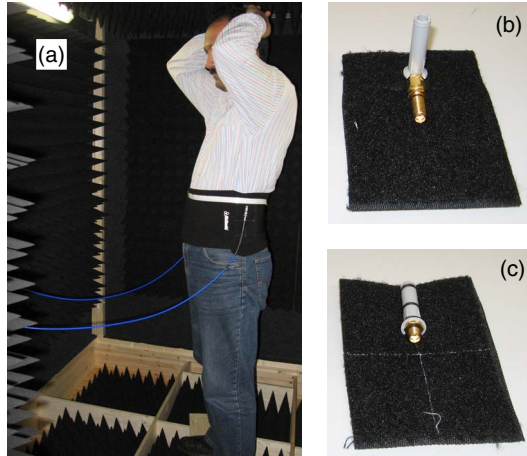
Fig. 1. Components for BAN measurements: (a) anechoic chamber with subject, (b) right-angle monopole antenna, (c) straight monopole antenna
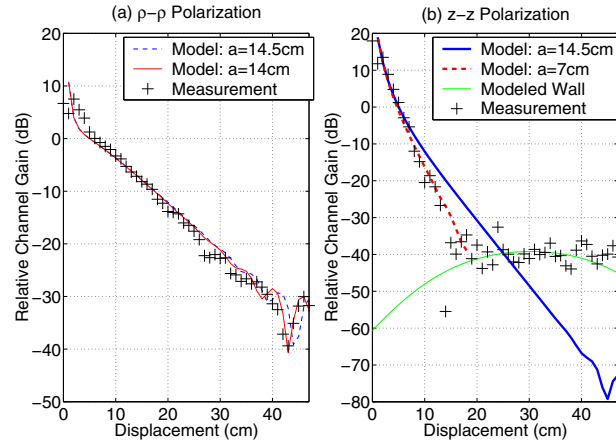

Fig. 2. Response of BAN channels for the cylindrical model compared with anechoic chamber measurements where the transmit and receive antennas were (a) $\hat{\rho}$ oriented, and (b) $\hat{z}$ oriented.

Figure 2(a) depicts the result for $\hat{\rho}$ oriented transmitter and receiver (antenna perpendicular to body), where measurements were taken using Setup A. The model is able to accurately predict the field decay with increasing separation, as well as the presence of a small dip just before the most extreme separation. This dip likely occurs due to partial cancellation of the two waves that propagate around the body in opposite directions, where the effect would mainly be seen when the waves have nearly equal amplitude (but opposite sign). The location of the dip is better matched by slightly reducing the radius in the model to 14 cm. The agreement is remarkable considering the simplicity of the model.

Figure 2(b) shows the result for $\hat{z}$ oriented transmitter and receiver (antenna parallel to body). This polarization exhibits very high shadowing due to the body, and Setup B was required to obtain better accuracy. Although the initial decay with increasing separation is captured by the model, The decay is not well predicted for larger separations. Apparently the $\hat{z}$ polarization is very sensitive to the level of curvature of the body surface, which is expected to be approximately ellipsoidal (not circular). Modeling the body with higher curvature using a smaller (but non-physical) radius of 7 cm gives better agreement.

Figure 2(b) also illustrates that a floor in the response is seen above 15 cm separation, apparently due to a specular wall reflection in the chamber. This was checked by computing fields radiated from the transmit antenna to an image of the receive antenna (on the opposite side of the wall) and adding an additional 40 dB of loss for the absorber. The resulting curve in Figure 2(b) is very close the the observed floor, suggesting that it is indeed due to the wall reflection. This observation indicates that performing BAN measurements for very shadowed conditions in compact anechoic chambers may be difficult, since wall reflections can easily overshadow on-body propagation mechanisms. Note that more efficient antennas or higher transmit power will not help, since both the on-body signal and the wall reflection would be increased. Overcoming this problem may require a larger chamber, cleverly placed or stronger absorbing material, time-gating of measurements, or a combination of these techniques.

V. CONCLUSION

This work investigated employing the analytical Green's function for a lossy cylindrical circular scatterer for body-only propagation modeling. Measurements were performed in a compact anechoic chamber using non-resonant monopole antennas. Results indicated that although good agreement is seen for $\hat{\rho}$-directed polarization, model predictions are less accurate for $\hat{z}$ polarization. It was also found that wall reflections in the anechoic chamber are actually still significant compared to on-body propagation for strongly shadowed cases.

REFERENCES

[1] A. Alomainy, Y. Hao, X. Hu, C. G. Parini, and P. S. Hall, "UWB on-body radio propagation and system modelling for wireless body-centric networks," *IET Proc. Commun.*, vol. 153, pp. 107–114, Feb. 2006.
[2] S. L. Cotton and W. G. Scanlon, "An experimental investigation into the influence of user state and environment on fading characteristics in wireless body area networks at 2.45 GHz," *IEEE Trans. Wireless Commun.*, vol. 8, pp. 6–12, Jan. 2009.
[3] A. Fort, F. Keshmiri, G. R. Crusats, C. Craeye, and C. Oestges, "A body area propagation model derived from fundamental principles: Analytical analysis and comparison with measurements," *IEEE Trans. Antennas Propag.*, vol. 58, pp. 503–514, Feb. 2010.